6
Formaldehyde gas sensing mechanism and Modelling

In this chapter, firstly, we will discuss about the formaldehyde gas sensing mechanism of pristine metal oxide SnO_2 and ZnO semiconductor materials. Next, we will discuss the effect of surface decoration on enhanced formaldehyde sensing using n-type ZnO and p-type NiO nanoparticles on pristine n-type SnO_2 due to the formation of n-n and p-n heterojunction. Secondly, other important parameters of NiO/SnO_2 sensor such as response time (τ_{res}), recovery time (τ_{rec}), surface coverage (θ) and adsorption (K_a) and desorption rate constant (K_d) were calculated from experimental data using Langmuir gas adsorption-desorption model via curve fitting method.

6.1 Discussion on formaldehyde gas sensing mechanism

6.1.1 Formaldehyde gas sensing mechanism of SnO_2 pristine metal oxide

It is well known that SnO_2 is n-type metal oxide semiconductor having a bandgap of 3.67 eV [Jing Cao, Ziying Wang, Rui Wang, Sen Liu, Teng Fei, 2015]. The gas sensing mechanism of SnO_2 metal oxide in the presence of reducing or oxidizing gas follows the surface-resistance controlled model. When the SnO_2 metal oxide material is heated above the operating temperature of 100°C, the free electrons are generated from its conduction band[Li et al., 2015b] [Li et al., 2019c]. When SnO_2 metal oxide sensor was exposed to atmospheric air, oxygen molecules come into contact of top surface of metal oxide gas sensing layer. The adsorbed oxygen molecules were converted into various types of chemisorbed oxygen ions (O_2^-, O^- or O^{2-}) at a different operating temperatures from 100-300°C by trapping electrons from its conduction band [Barsan et al., 2002; Korotcenkov, 2007] as shown in figure 6.1 (a). The reaction mechanisms to form O_2^-, O^- or O^{2-} ions at various temperatures are summarized as follows [Khamfoo et al., 2020]:

$$O_{2\,(gas)} \leftrightarrow O_{2\,(ads)} \tag{6.1}$$

$$O_{2(ads)} + e^- \leftrightarrow O_{2\,(ads)}^- \quad (T < 100°C) \tag{6.2}$$

$$O_{2\,(ads)}^- + e^- \leftrightarrow 2O_{(ads)}^- \quad (100°C < T < 200°C) \tag{6.3}$$

$$O_{(ads)}^- + e^- \leftrightarrow O_{(ads)}^{2-} \quad (T > 200°C) \tag{6.4}$$

At a lower operating temperature of 100°C, in the atmospheric air, the oxygen molecules react with generated electrons from the conduction band of material and form O_2^- ions. After increasing the temperature in the sensing layer in the range of 100°C < T <200°C, O_2^- ions react with more electrons and form the O^- ions. Here, the O^- ions play the main dominating role on the top surface of n-type SnO_2 materials during the reaction with target gases. As the formation of O_2^-, O^- or O^{2-} chemisorbed oxygen ions on the top surface of n-type SnO_2 materials, the electron concentration in the conduction band of SnO_2 materials has been reduced. As a results, the resistance of the SnO_2 materials has increased and a space-charge region has been formed as the O_2^-, O^- or O^{2-} chemisorbed oxygen ions repeal the electrons in the surface of the SnO_2 materials as shown in figure 6.1 (a) and 6.2 (a) [Castro-Hurtado et al., 2013]. During the test, in the presence of reducing gas (HCHO), a chemical reaction has occurred between the adsorbed oxygen ions (O_2^-, O^- or O^{2-}) at the SnO_2 grains boundaries and formaldehyde gas as shown in figure 6.1 (b) and 6.2 (b). As a result, $CO_{2(gas)}$, $H_2O_{(gas)}$ and $HCOOH_{(gas)}$ were produced as a byproduct and electrons (e^-) were released back to the conduction band of the metal oxide (SnO_2) sensing layer as shown in equation (6.5) and (6.6). Generally, the oxidation of formaldehyde gas governs the process of gas detection during the test. In the following equations (6.5) and (6.6), we have discussed the possible oxidation reactions which happen between the formaldehyde gas and the adsorbed oxygen ions [Dong et al., 2015]:

$$HCHO_{(ads)} + 2O^-_{(ads)} \rightarrow CO_{2(gas)} + H_2O_{(gas)} + 2e^- \quad (6.5)$$

$$HCHO_{(ads)} + O^-_{(ads)} \rightarrow HCOOH_{(gas)} + e^- \quad (6.6)$$

In the first reaction, water and carbon dioxide were produced, which are shown in equation (6.5) and in the second reaction (equation (6.6)), formic acid was produced. Hence, after reaction with HCHO gas, the concentration of electrons in the conduction band also has been increased and so, the conductivity of SnO_2 sensing layer materials has been increased [Tiemann, 2007] as shown in figure 6.1 (b).

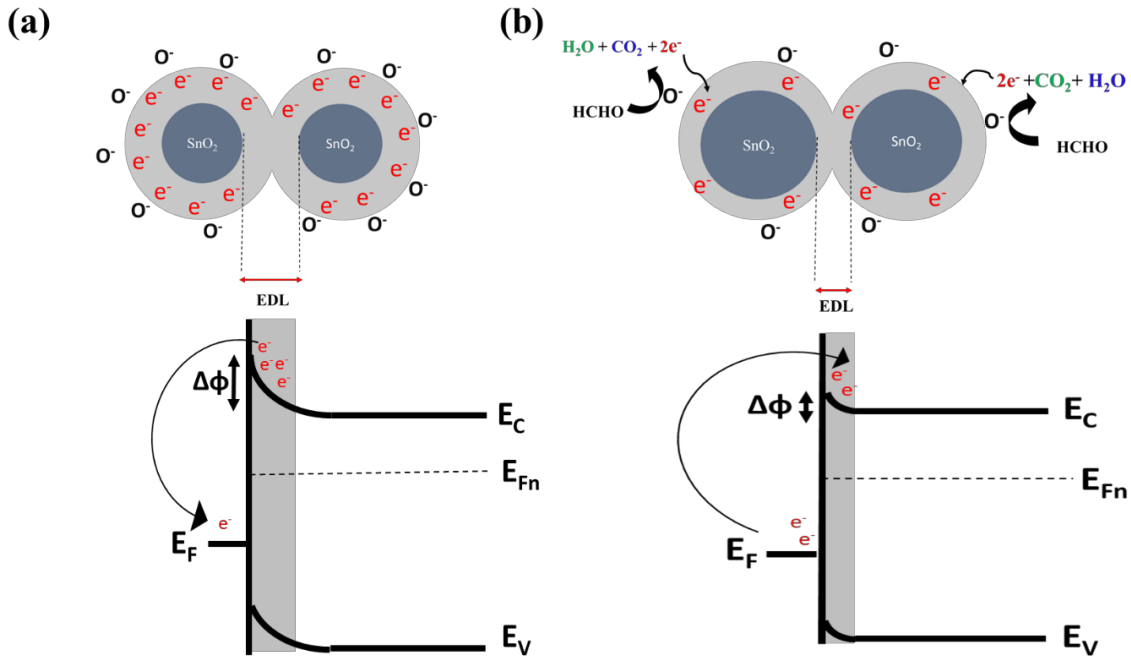

Figure 6.1: HCHO sensing mechanism on SnO_2 surface. (a) Adsorbed O_2 molecules take out electrons from SnO_2 which leads to the generation of the EDL. (b) HCHO gas reacts with adsorbed O^- ions on the SnO_2 surface, releasing electrons that are reinjected in the conduction band and decrease in EDL.

The reaction of formaldehyde gas with adsorbed oxygen molecules in SnO_2 surface is shown in figure 6.2 (b) via a schematic diagram.

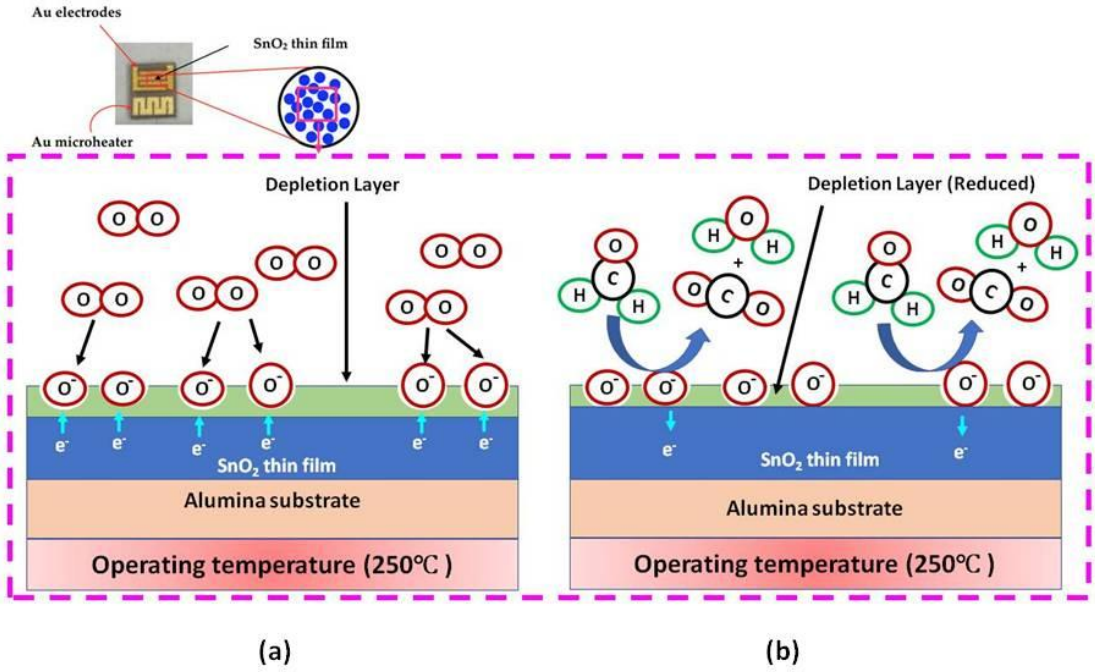

Figure 6.2: Schematic diagram of the SnO_2 sensing layer (a) in the presence of oxygen and (b) in the presence of formaldehyde gases.

6.1.2 Formaldehyde gas sensing mechanism of ZnO pristine metal oxide

It is well reported that ZnO is a typical n-type metal oxide semiconductor (bandgap 3.37 eV) and the ZnO sensing film shows its optimum response towards formaldehyde gases via the surface-resistance controlled model. It was observed in FESEM images that the obtained laser ablated ZnO nanoparticles were highly porous and it had high gas adsorption sites having a huge number of oxygen vacancies (V_o) which ionizes to form donor energy levels. The schematic diagram (Figure 6.3) shows the change in resistance when the ZnO nanoparticles are exposed to formaldehyde (HCHO) gas. When the ZnO material was heated (100°C - 300°C), free electrons were generated in the surface from the conduction band of ZnO and oxygen molecules were chemisorbed as a O_2^-, O^- or O^{2-} ions on the surface by trapping electrons from its conduction band. Formation of O_2^-, O^- and O^{2-} ions occurred at different temperatures from 100°C - 300°C, the atmospheric oxygen molecules (O_2) are adsorbed on ZnO NPs surface. At lower temperatures (T < 100°C), free electrons on the surface of ZnO nanomaterials are captured by the oxygen molecules (O_2) to form O_2^- ions, as shown in figure 6.3 and equation (6.2). Further, at higher temperatures (T > 100°C), O_2^- ions again combined with the free electrons and formed O^- ions.

Furthermore, when the sensing layer temperature further increases above 200°C, the O^- ions was formed into O^{2-} ions. Thus, a depletion layer was formed due to the accumulation of chemisorbed oxygen ions (O_2^- , O^- or O^{2-}) on the surface of the ZnO materials. As a result, the resistance of the sensing films was increased. When the ZnO nanoparticles based sensor was exposed to formaldehyde gas, the reaction were occurred between formaldehyde and the adsorbed oxygen ions (O_2^-, O^- or O^{2-}). During the reaction, CO_2 (g), H_2O (g) were produced and electrons (e^-) were also generated which were released back to the conduction band. As the electrons were transferred back into the conduction band of the ZnO surface, the resistance of ZnO materials was decreased. The possible reactions to happen with formaldehyde gas via adsorbed oxygen ions are shown in the equation (6.5) and (6.6).

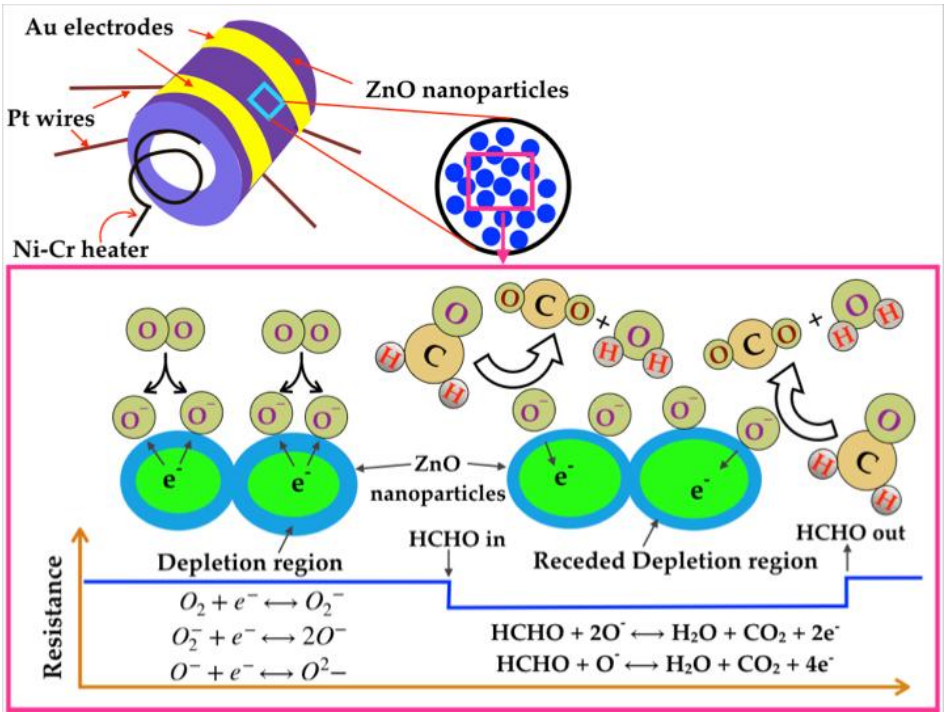

Figure 6.3: Schematics of HCHO gas sensing mechanism using ZnO nanoparticles.

6.1.3 Formaldehyde gas sensing mechanism of ZnO/SnO_2 n-n heterojunction

When the ZnO/SnO_2 sensor was exposed to atmospheric air at higher working temperature (> 100°C), the free electrons of n-type SnO_2 and ZnO react with oxygen species and chemisorbed oxygen ions (O_2^-, O^- or O^{2-}) were formed on the top surface of SnO_2 and ZnO layer as shown in figure 6.4 (b). Figure 6.4 (a) and (d) shows the band diagram of the ZnO/SnO_2 heterojunction sensor before and after contact. Formaldehyde gas sensing mechanism with schematic diagrams are shown in figure 6.4 (b) and (c). From the figure 6.4 (a) it can be seen that Fermi energy level of SnO_2 is higher than that of ZnO as the electron affinity (χ) of SnO_2 is 4.2 eV, while the electron affinity (χ) of ZnO is 4.5 eV. Hence, after contact formation between SnO_2 and ZnO after surface decoration, electrons from the conduction band of n-type SnO_2 flow to the conduction band of n-type ZnO to match the Fermi levels. Due to reduction of free electrons in the n-type SnO_2, the conduction band of the n-type SnO_2 side will bend upwards as two Fermi levels try to reach the same energy level, as shown in figure 6.4 (d). As a results, the potential barrier and thickness of electron depletion layer (EDL) of ZnO/SnO_2 sensor have been increased and due to this effect, the resistance of the sensor has been increased (Figure 6.4 (b) and (d)). As we seen that in air, the baseline resistance (R_a) of pristine SnO_2 sensor was 0.75 MΩ (T_{op} = 300°C), while ZnO nanoparticles decorated on SnO_2 sensor was 1.7 MΩ (T_{op} = 250°C). The change of baseline resistance (R_a) of ZnO/SnO_2 sensor was occurred due to the potential barrier and formation of electrons depletion layer (EDL) [Chang et al., 2018a][Ren et al., 2015].

From the test results, it was observed that SnO_2 and ZnO/SnO_2 sensors are both sensitive to HCHO. But, the response of ZnO/SnO_2 heterojunction based sensors is higher than pristine SnO_2 sensors. Thus, gas adsorption active sites of ZnO/SnO_2 were greatly enhanced by the surface modification of SnO_2 with laser ablated ZnO nanoparticles. Moreover, the enhanced response of ZnO/SnO_2 heterojunction based sensors can be described as follows: Laser ablated ZnO nanoparticles have a huge amount of oxygen vacancy (V_o), and, large no of active surface adsorption sites with porosities. Furthermore, three types of junction boundaries exist in ZnO/SnO_2 composite structure: the boundaries between n-SnO_2 - n-SnO_2 (n-n) homogeneous crystallites, n-ZnO - n-ZnO (n-n) homojunctions and the heterogeneous crystallites between n-SnO_2 and n-ZnO (n-SnO_2/n-ZnO heterojunctions) [Wang et al., 2013]. As a result, more target gas molecules interact with chemisorbed oxygen molecules (O_2^-, O^- or O^{2-}) and more captured

electrons will be released back to the gas sensing materials [Barsan et al., 2001b]. During the exposure of ZnO/SnO_2 sensors in formaldehyde gas, the reaction between formaldehyde and the adsorbed oxygen ions (O_2^-, O^- or O^{2-}) produces CO_2 (g), H_2O (g) and electrons (e^-). Figure 6.4 (e) shows the schematic diagram of energy band model of the n-ZnO/n-SnO_2 heterostructure during reaction of formaldehyde with adsorbed O_2 molecules at thermal equilibrium. The released electrons were returned back to the sensor surface, and hence, nanocrystallities boundary barrier of hetero-junction (n-type SnO_2/n-type ZnO) was reduced, as shown in figure 6.4 (c) and (e). The resistance of the ZnO/SnO_2 sensors was reduced. Thus ZnO/SnO_2 heterojunction based sensor exhibited much higher response to formaldehyde compared to the pristine SnO_2 sensor.

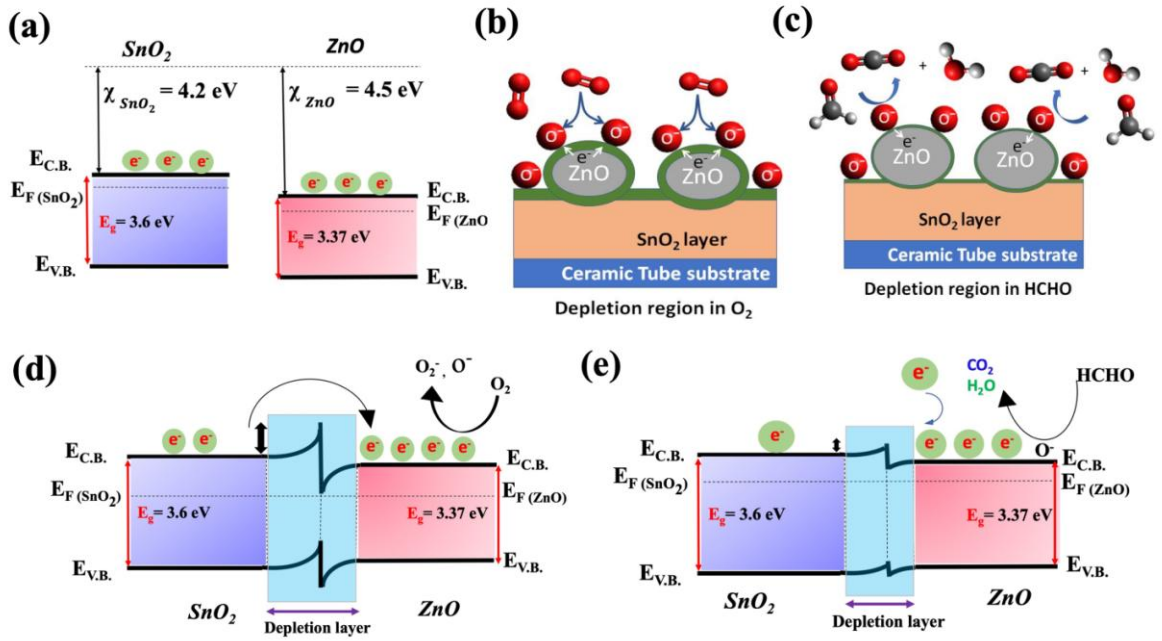

Figure 6.4: (a) Proposed energy band diagram of n-type SnO_2 and n-type ZnO heterojunctions before contact. (b) and (d) Schematic illustration of ZnO/SnO_2 heterostructure in air after contact formation at thermal equilibrium. (c) and (e) Reduced depletion layer of ZnO/SnO_2 heterostructure during the reaction of HCHO vapor with adsorbed O_2 molecules after contact formation at thermal equilibrium. E_c : lower level of the conduction band, E_F : Fermi level and E_v : upper level of the valence band.

6.1.4 Formaldehyde gas sensing mechanism of NiO/SnO_2 p-n heterojunction

The gas-sensing mechanism fully depends on the chemical adsorption/desorption process of oxygen on the surface of metal oxide materials according to the Langmuir adsorption model[Vuong et al., 2015]. Free electron is generated due to the heating of n-type SnO_2 thin film and at higher temperatures (>100°C), oxygen molecules are dissociated via chemisorption process[Barsan et al., 2001a] and it is connected via dipole bonding to the semiconductor surface atoms as shown in figure 6.5 (a). Under this condition, the electron is transferred from the conduction band of the semiconductor surface to the adsorbed oxygen and forms an electron depletion layer (EDL) beneath the surface of n-type SnO_2 sensing layer (Figure 6.5 (a)). As a result, the resistance of the sensing layer has been increased. On the other hand, in the presence of HCHO vapor, the chemisorbed oxygen ions (O^{2-} and O^-) easily reacts with HCHO and produce water, CO_2 and release electrons to the conduction band as shown in Figure 6.5 (b)[Meng et al., 2018a]. Hence, the resistance has been decreased by the higher concentration of electron in the surface.

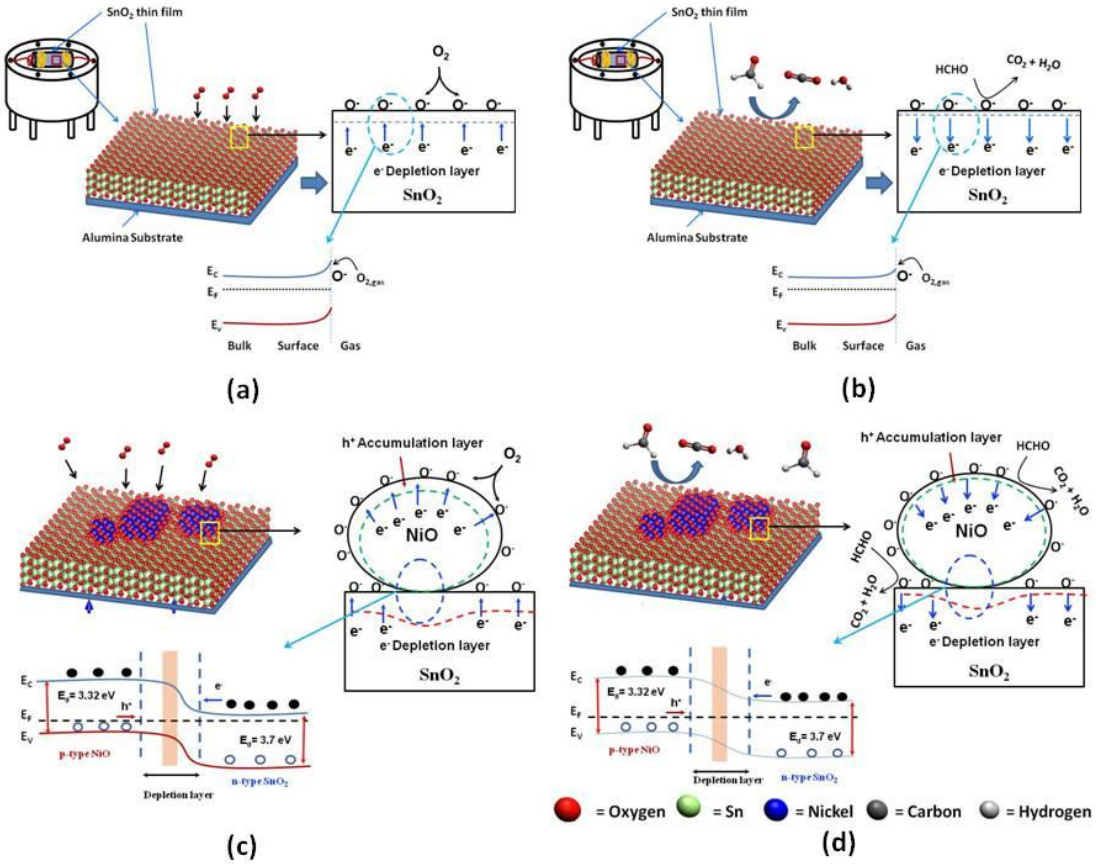

Figure 6.5 : Schematic band diagram of pristine SnO_2 thin film in the presence of (a) oxygen and (b) HCHO. Schematic band diagram of NiO/SnO_2 sensor in the presence of (c) oxygen and (d) HCHO.

On the other hand, after the heating of NiO sensing layer, the resistance of p-type NiO has been decreased due to the increase of hole concentration underneath the NiO surface[Fang et al., 2017]. As compared with pure SnO_2, the baseline resistance (R_a) of NiO decorated SnO_2 sensor has been increased by ~ 2.4 times at optimum operating temperature at 210°C in air. The same phenomenon, changes of resistance after decoration has been observed by other researchers[Ju et al., 2015][Fang et al., 2017]. In *p*-NiO/*n*-SnO_2 composite structure, three types of junctions have been formed [Jin et al., 2021][Du et al., 2012]: *p*-NiO/ *p*-NiO homojunctions, *n*-SnO_2 /*n*-SnO_2 homojunctions and *p*-NiO/*n*-SnO_2 heterojunctions. *p*-NiO/*n*-SnO_2 heterojunctions are closely associated with improved sensing performance and the schematic diagram is shown in figure 6.5 (c). Figure 6.5 (c) shows the energy band diagram of the *p*-NiO/*n*-SnO_2 grains in ambient air. After the formation of p-n heterojunction, the majority charge carrier in SnO_2 is electrons move to the *p*-NiO and the holes (majority charge carriers in p-type NiO) are transferred to equal the Fermi level. As a result, band bending occurred, thus creating a potential barrier as shown in Figure 6.5 (c). Thus, potential barrier and EDL contribute the change of resistance in composite structures. When the *p*-NiO/*n*-SnO_2 sensor was exposed to HCHO vapor, the depletion layer was reduced, as shown in figure 6.5 (d) and the energy band diagram of *p*-NiO/*n*-SnO_2 grains boundary area in the presence of reducing gas formaldehyde is shown in figure 6.5 (d). The reducing gas HCHO easily reacts with surface chemisorbed oxygen ions (O^{2-} and O^-) and produces water, CO_2 and releases electrons to the conduction band. The resistance has been decreased by the higher concentration of electron in the surface. The byproduct water vapor on the surface of the sensing layer takes time to desorbed completely which affects the recovery time of the sensor.

The *p*-NiO/*n*-SnO_2 sensor showed excellent gas sensing performance to formaldehyde due to the nano-size effect of laser ablated NiO NPs which adsorbed more oxygen molecules which helped to react with adsorbed ionized oxygen molecules with HCHO gas.

6.2 Gas sensor modelling

6.2.1 Gas adsorption-desorption kinetics in metal oxide

When the metal oxide sensing layer is heated, the oxygen molecules adsorb on the metal oxide surface via the following reaction [Becker et al., 2001]:

$$O_2\,(g) + e^- \leftrightarrow O_2^-\,(ads) \qquad (6.7)$$

In the metal oxide sensor, we assumed that the total number of adsorption sites density on the metal oxide surface for molecular gas adsorption is N_{tot} which is directly proportional to the available surface area of metal oxide. During the gas sensing performance test, a reaction occurred between formaldehyde gases and the adsorbed oxygen molecules. The adsorption rate constant (K_a) of analyte gas formaldehyde is proportional to the concentration of analyte molecules (C_a) and the empty adsorption sites ($N_{tot} - N_{occ}(t)$). The desorption rate constant (K_d) is proportional to the occupied adsorption sites N_{occ}. According to the proposed Langmuir adsorption model as discussed in Ref. [Vuong et al., 2015][Lee et al., 2005], the rate of change of occupied adsorption sites can be described as :

$$\frac{dN_{occ}(t)}{dt} = K_a\,[N_{tot} - N_{occ}(t)]C_a - K_d N_{occ}(t) \qquad (6.8)$$

After solving the first-order differential equation with boundary condition (at t = 0)

$$N_{occ}(t) = \left[\frac{K_a\,C_a\,N_{tot}}{K_a C_a + K_d}\,\left(1 - \exp\left(-\frac{t}{\tau_{res}}\right)\right)\right] \qquad (6.9)$$

$$\text{where } \tau_{res} = \frac{1}{C_a K_a + K_d} \quad = \text{ Response time of sensor} \qquad (6.10)$$

the rate of adsorption is exactly counter balanced by rate of desorption. So $\frac{dN_{occ}(t)}{dt} = 0\ at\ t = \infty$. The surface coverage ($\theta$) by the analyte gas phase in the metal oxide as per Langmuir adsorption is as follows:

$$\theta = \frac{K_a\,C_a}{K_a\,C_a + K_d} = \frac{K^{eq}}{K^{eq}+1} \qquad (6.11)$$

$$\text{Where } K^{eq} = \frac{K_a}{K_d} \quad = \text{ The equilibrium rate constant} \qquad (6.12)$$

The equilibrium rate constant (K^{eq}) depends on the operating temperature of sensor. In the recovery process the desorption rate is given by

$$\frac{dN_{occ}(t)}{dt} = -K_d N_{occ} \qquad (6.12)$$

$$N_{occ}(t) = \frac{K_a\,C_a}{K_a\,C_a + K_d}\,exp(-K_d t) = \frac{K_a\,C_a}{K_a\,C_a + K_d}\,exp\left(-\frac{t}{\tau_{rec}}\right) \qquad (6.13)$$

$$\text{where } \tau_{rec} = \frac{1}{K_d} = \text{Sensor recovery time} \qquad (6.14)$$

6.2.2 Changes in conductance of sensor due to adsorption-desorption of gases

Electrons capture or release from the top of the metal oxide surface due to the analyte gas adsorption or desorption process. As a result, an electron depletion layer (EDL) has been formed. Due to the electron capture or release, the conduction of the metal oxide has been changed. Thus, time-dependent response conductance change as follows :

$$\Delta g(t) = \Delta g_{max}\left[1 - exp\left(-\frac{t}{\tau_{res}}\right)\right] \text{ for response cycle} \qquad (6.15)$$

Where $\Delta g(t)$ = Change of conductance of the sensor with time

Δg_{max}= maximum change of conductance of the sensor

$$\Delta g(t) = \Delta g_{max} exp\left(-\frac{t}{\tau_{rec}}\right) \text{ for recovery cycle} \qquad (6.16)$$

the value of τ_{res} and τ_{rec} can be obtained from the fitting of the sensor response and recovery curves.

6.2.3 Transient response-recovery cycles with fitting curve of pristine SnO_2 sensor

The experimental response and recovery cycles with the fitting curves of SnO_2 sensors for different concentrations (0.5 to 50 ppm) are shown in figure 6.6 and 6.7, respectively. It can be seen in figure 6.6 that after injection of analyte HCHO vapor into the test chamber, sensing layer conductance was increased exponentially due to the presence of reducing gas and sensor reached its steady state saturation level within seconds for a particular concentration of HCHO. After opening the test chamber to ambient air, the sensor conductance reaches to its original baseline level, as shown in figure 6.7. Fitting curves are shown in each figure by a dashed red colour line for each concentration level. It is clearly observed in figure 6.6 and 6.7 that no significant deviation has been observed between the experimental data and fitting curve. Figure 6.8 (a) and (b) summarize the normalized conductance change ($\Delta g/\Delta g_{max}$) as a function of time during response and recovery of SnO_2 sensor to various concentrations of HCHO vapor at 300°C. The response and recovery fitting curve due to 50 ppm HCHO concentration is shown in figure 6.8 (a) by dashed line.

The kinetic parameters response (τ_{res}) and recovery (τ_{rec}) time of the sensor are very important parameters to estimate the sensing performance for on-site detection. The response time is defined as the time required for the sensor to reach 90% of the equilibrium value in the presence of HCHO and recovery time is defined as the time required for a sensor to recover 10% lower than its original baseline value. As per the equation (6.9), response time (τ_{res}) varies with analyte gas (HCHO) concentration (C_a). The original response time (τ_{res}) of the sensor was measured via the fitting curve in each normalized time-dependent response graph as shown in figure 6.6. The value of response time (τ_{res}) was 17 s to 8 s in the examined HCHO concentration range of 0.5 to 50 ppm. It was found that the response time was shorter for higher concentrations, as expected from equation (6.9).

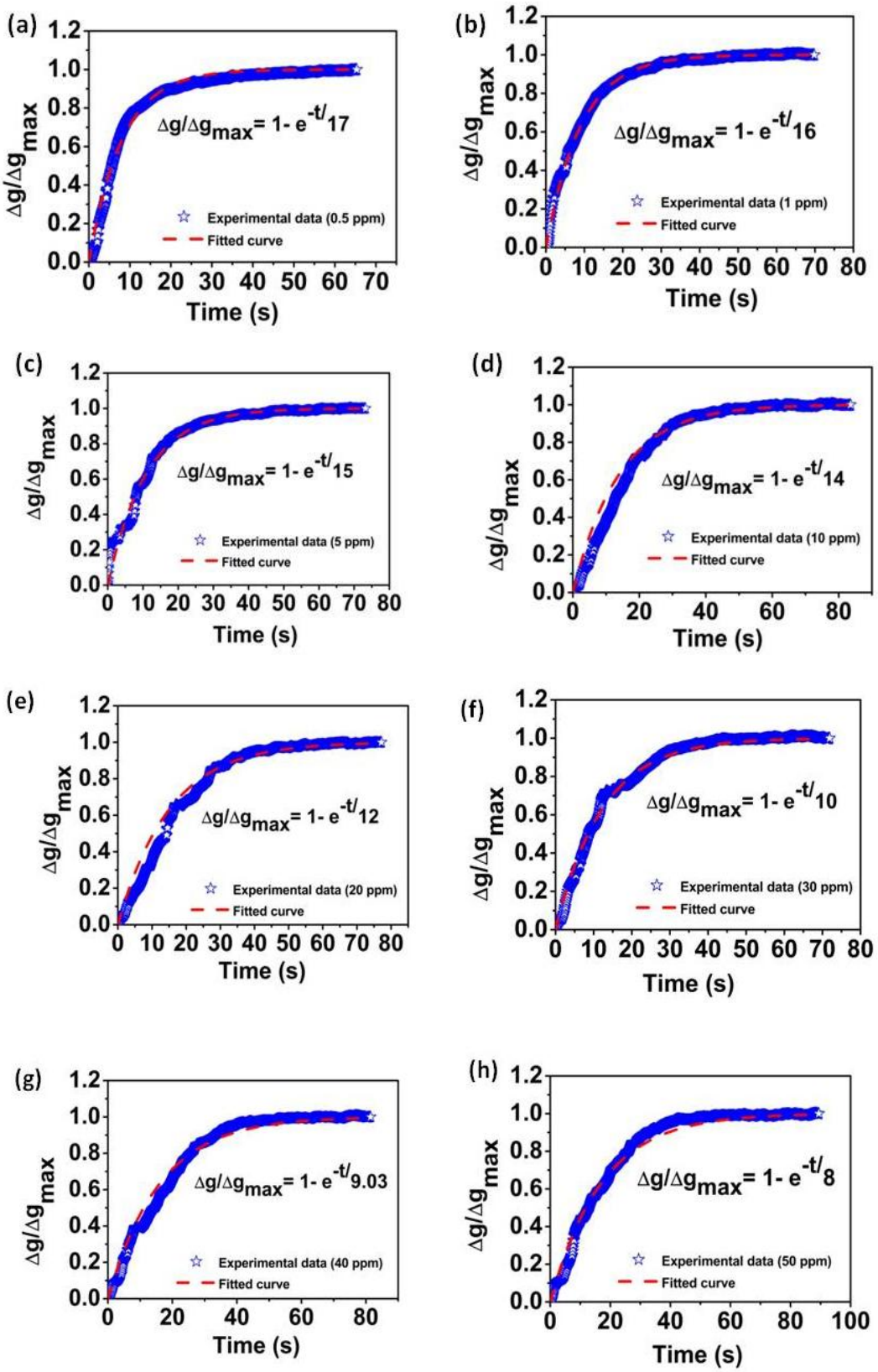

Figure 6.6 : Response behaviour of pristine SnO_2 sensor for different concentration of HCHO (0.5, 1, 5, 10, 20, 30, 40 and 50 ppm). The fitting lines are shown in the figure by a red colour dashed line.

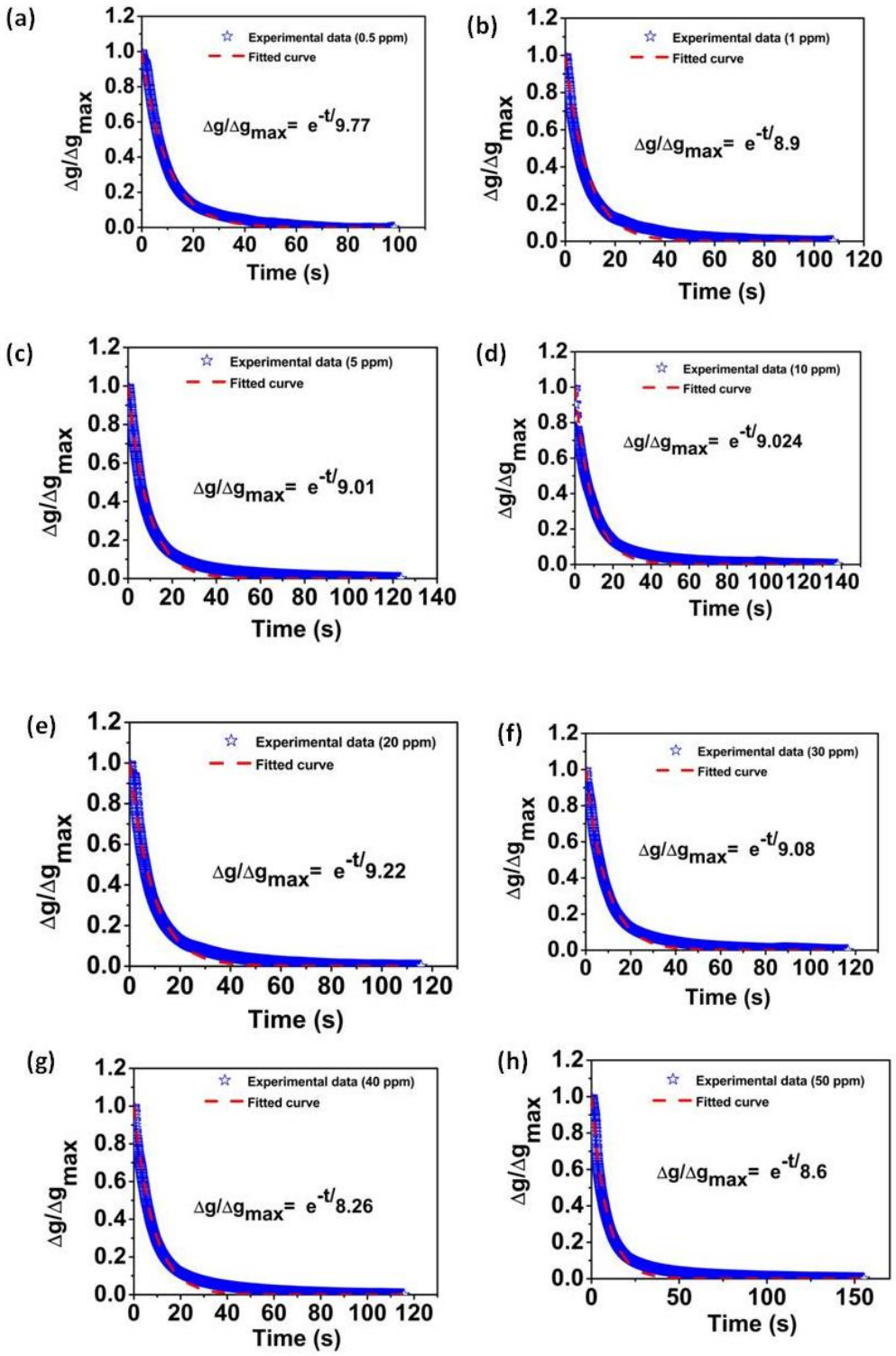

Figure 6.7 : Recovery behaviour of pristine SnO_2 sensor for different concentrations of HCHO (0.5, 1, 5, 10, 20, 30, 40 and 50 ppm). The fitting lines are shown in the figure by a red colour dashed line.

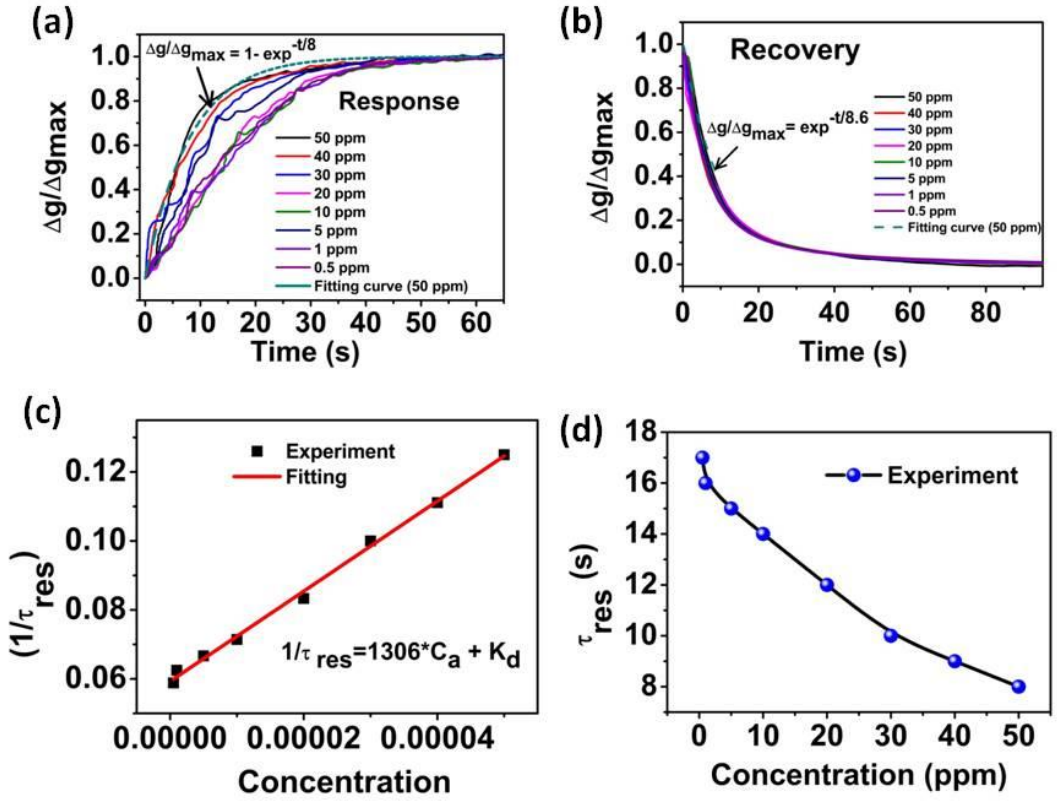

Figure 6.8: (a) Summarization of normalized response curves of SnO_2 sensor towards different concentrations of HCHO range 0.5 ppm to 50 ppm at 300°C. (b) Summarization of normalized recovery curves of SnO_2 sensor towards different concentrations of HCHO range 0.5 ppm to 50 ppm at 300°C. (c) $1/\tau_{res}$ vs. HCHO concentration of SnO_2 to obtain the K_a value. (d) τ_{res} vs. HCHO concentration.

Furthermore, recovery time (τ_{rec}) is independent of the analyte gas (HCHO) concentration (C_a), as shown in equation (6.14). All the desorption curves are shown in figure 6.7 for various HCHO concentrations. The recovery time (τ_{rec}) can also be obtained from the sensor recovery experimental data via a fitting curve for a fixed HCHO concentration. The summarized recovery curves in figure 6.8 (b) clearly prove that the desorption rate is independent of the gas concentration as we seen in equation (6.14). The calculated desorption time is 8.6 s which was almost constant for all concentrations of HCHO vapors.

Figure 6.8 (c) shows the plot $1/\tau_{res}$ as a function of the concentration of HCHO vapors. For pure SnO_2 sensor which leads to the estimation of K_a and K_d from equation (6.9). We have observed from figure 6.8 (c) that the $1/\tau_{res}$ of SnO_2 sensors increases almost linearly with increasing concentration of HCHO vapor from 0.5 to 50 ppm. In addition, the adsorption rate constant (K_a) can be measured from a series of measurements with varying HCHO concentration C_a. . The K_a value of the SnO_2 sensor obtained from the linear fit model in Figure 6.8 (c) was 1306 cm^3/s whereas desorption rate constant (K_d) can be obtained from the recovery graph of equation (12). K_d value of 0.1 was obtained from the recovery graph. The extracted value K_a and K_d are tabulated in Table 6.1. The equilibrium rate constant K^{eq} was 13060 (Table 6.1). So the detection limit of HCHO gas of the sensor SnO_2 sensor is $1/K^{eq} \sim 7.65e^{-3}$ %. The τ_{res} plot of sensor against HCHO concentration for SnO_2 sensor is shown in figure 6.8 (d).

We also calculated the value of surface coverage (θ) which is the ratio of the number of adsorption sites over the total adsorption sites. The surface coverage (θ) varies with gas concentration and is tabulated in Table 6.1 for specified gas concentration.

Table 6.1 : Summary of various parameters obtained from the fitting curve for SnO_2

Test Gas	K_a (cm^3*s^{-1})	K_d (s^{-1})	K_{eq}	Values at a concentration			
				C_a (Fraction)	τ_{res} (s)	τ_{rec} (s)	θ
HCHO	1306	0.1	13060	$5e^{-5}$	9	10	0.40

6.2.4 Transient response-recovery cycles with fitting curve of p-NiO/n-SnO_2 sensor

The experimental response and recovery cycles with the fitting curve of NiO/SnO_2 sensor are shown in the supporting information figure 6.9 and 6.10, respectively. From figure 6.9, the response times of NiO/SnO_2 sensor were calculated from the fitting curve and the range of response time was 5 to 1.7 s. From the fitting curve in figure 6.9 the recovery times were also measured and the value was in the range of 40 to 103.5 s for various HCHO concentration range. All the response graphs were summarized in figure 6.11 (a) and the green color dashed line in figure 6.11 (a) represents the fitting curve for 40 ppm HCHO concentration. All the recovery curves were summarized in figure 6.11 (b) and in this case, multiple recovery lines were observed and the recovery time is higher than the pristine SnO_2 sensor. During the recovery of NiO/SnO_2 sensor, the recovery time was 10 times more (102 s) than the SnO_2 sensor. The $1/\tau_{res}$ plot with respect to HCHO concentration, as shown in figure 6.11 (c), estimated the K_a value to be 7377 and K_d value obtained from the figure 6.11 (c) was 0.01. After calculation, K^{eq} value was obtained for NiO/SnO_2 737700 which is high compared to SnO_2 sensor, as shown in Table 6.2. So the detection limit of HCHO gas of the sensor SnO_2 sensor is $1/K^{eq} \sim 1.35e^{-6}$ %. The estimated steady state surface coverage (θ) is 97% at 50 ppm (Table 6.2). The surface coverage value of NiO/SnO_2 sensor during the reaction of HCHO is greater than the surface coverage of pristine SnO_2 sensor.

So, the limit of detection (LoD) of NiO/SnO_2 is $1.35e^{-6}$ % which is lower than our previously made SnO_2 sensor. From this comparison, the present NiO/SnO_2 sensors exhibit an obvious advantage over pure SnO_2 sensors.

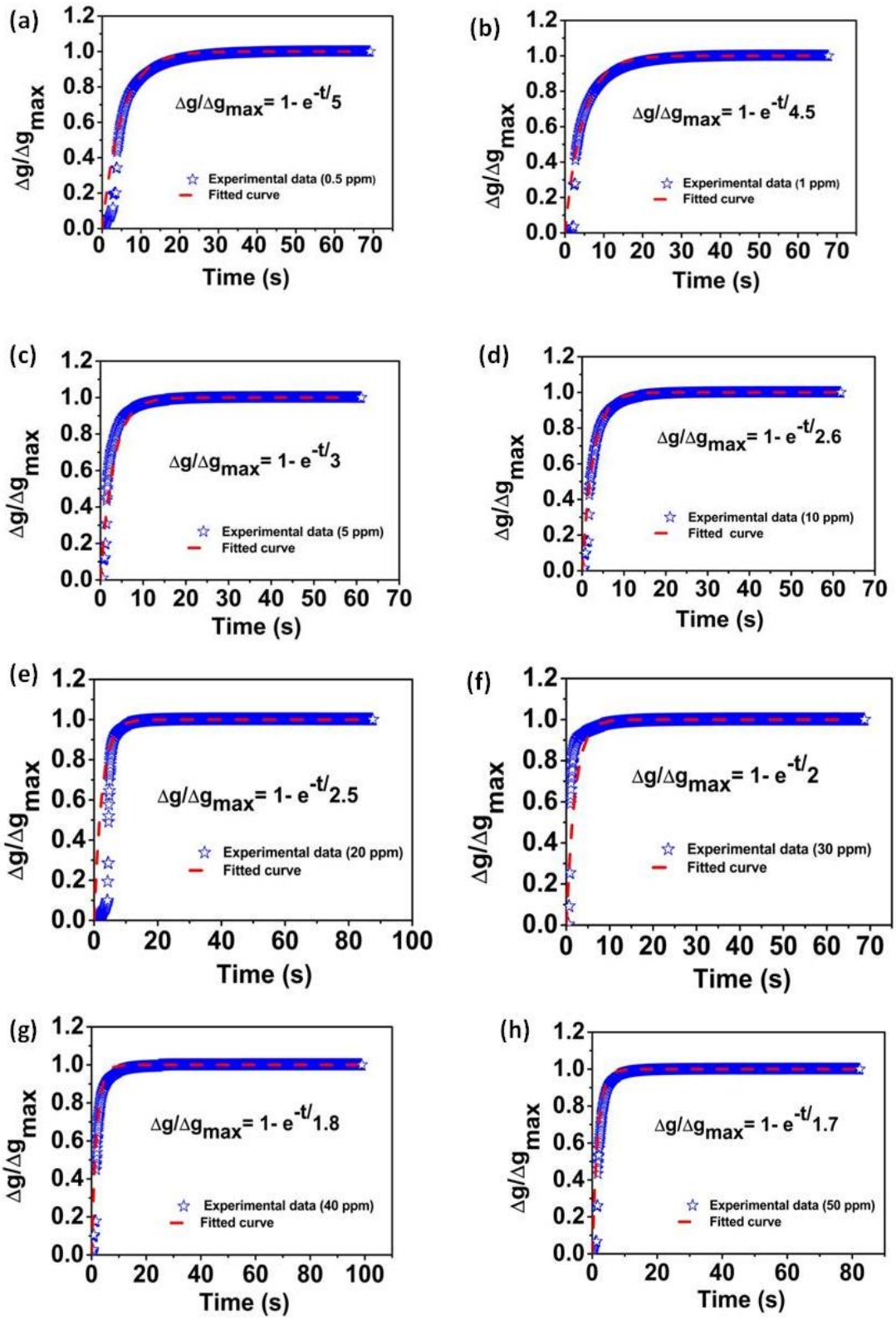

Figure 6.9 : Response behaviour of NiO/SnO_2 sensor for different concentrations of HCHO (0.5, 1, 5, 10, 20, 30, 40 and 50 ppm). The fitting lines are shown in the figure by a red colour dashed line which was used to extract the response time of sensors towards HCHO.

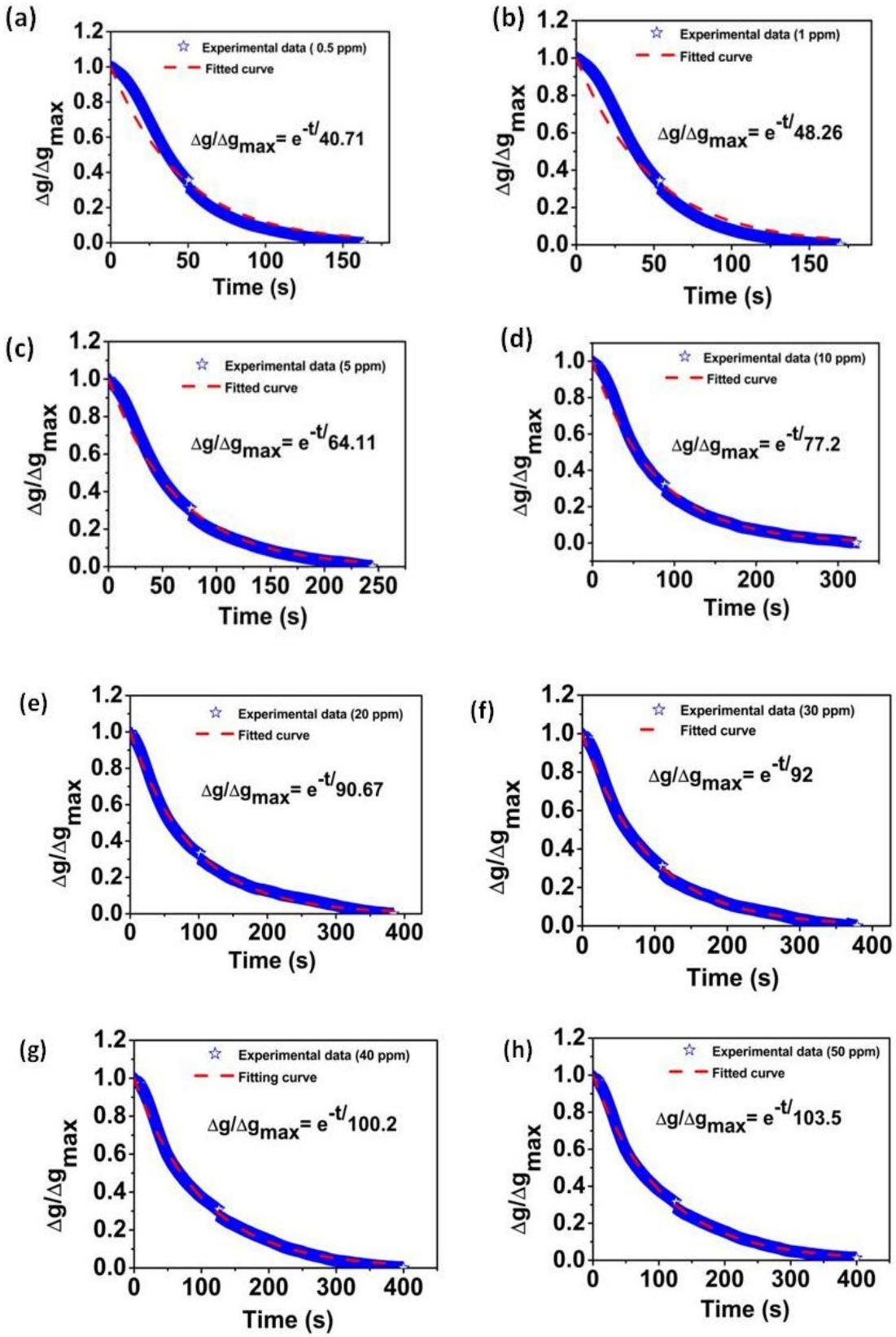

Figure 6.10 : Recovery behaviour of NiO/SnO_2 sensor for different concentrations of HCHO (0.5, 1, 5, 10, 20, 30, 40 and 50 ppm). The fitting lines are shown in the figure by a red colour dashed line which was used to extract the recovery time of sensors towards HCHO.

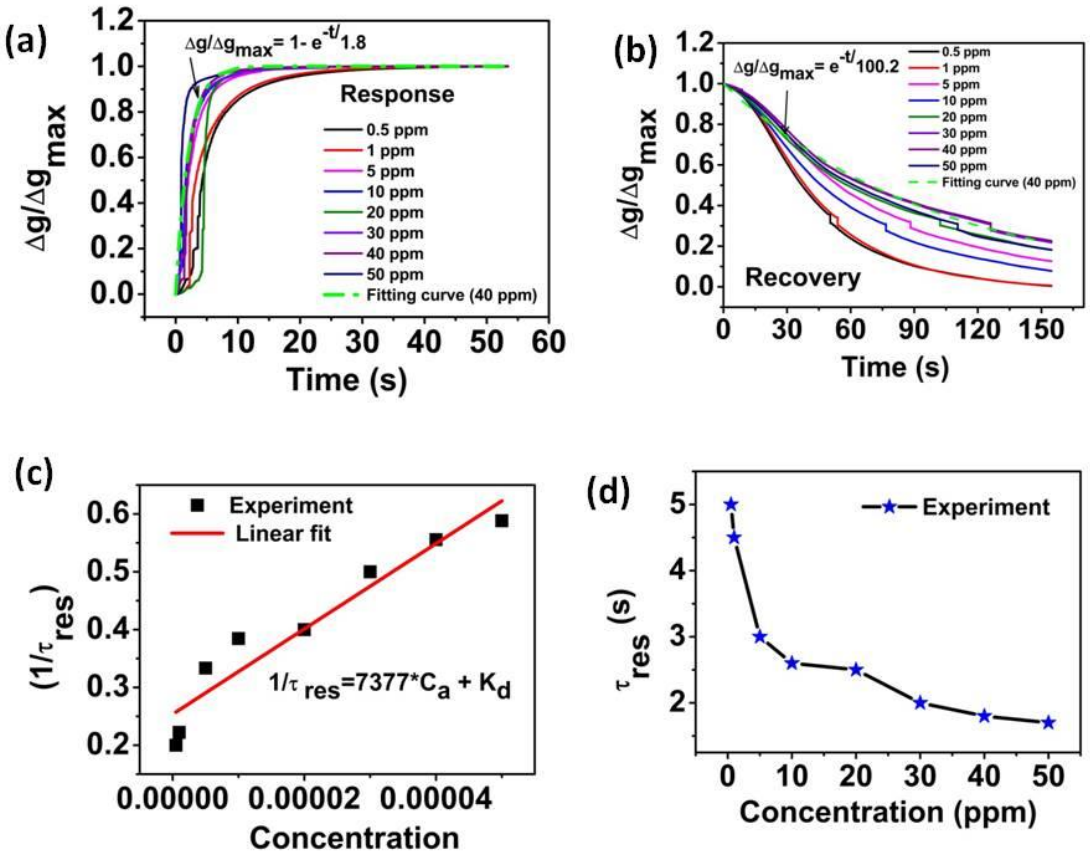

Figure 6.11 : (a) Summarization of normalized response curves of NiO/SnO_2 sensor towards different concentrations of HCHO range 0.5 ppm to 50 ppm at 210°C. (b) Summarization of normalized recovery curves of NiO/SnO_2 sensor towards different concentrations of HCHO range 0.5 ppm to 50 ppm at 210°C. (c) Linear fit model of NiO/SnO_2 sensors $1/\tau_{res}$ vs. HCHO concentration to obtain the K_a value. (d) τ_{res} vs. HCHO concentration of NiO/SnO_2 sensor.

Table 6.2 : Summary of various parameters obtained from the fitting curve for NiO/SnO_2

Test Gas	K_a (cm^3*s^{-1})	K_d (s^{-1})	K_{eq}	Values at a concentration			
				C_a (Fraction)	τ_{res} (s)	τ_{rec} (s)	θ
HCHO	7377	0.01	737700	$5e^{-5}$	1.7	100.2	0.97

6.3 Conclusion

We have studied the formaldehyde gas sensing mechanism of pristine (SnO_2, ZnO) and heterojunction based (ZnO/SnO_2 and NiO/SnO_2) sensors. We have also understood the enhanced formaldehyde sensing mechanism of heterojunction based sensors due to the formation of depletion layer via the heterojunctions on the sensing material surface. A simple Langmuir-Hinshelwood was developed to find the adsorption and desorption rate constants of the gas molecules on the surface of the gas sensor. The Langmuir gas adsorption-desorption model demonstrated the irreversible type of gas sensing behaviour towards HCHO as the response time of the sensor is disproportionately lowered with the increase in HCHO concentration. The forward rate constant (K_a) of p-NiO/n-SnO_2 is 5.6 times more than compared to SnO_2 gas sensor obtained using L-H model. The surface coverage value (θ) of NiO/SnO_2 sensor is 14.25% greater than the pristine SnO_2 sensor with the 50 ppm of HCHO gas concentration. Extraction of various gas sensing parameters via modelling is a very useful technique for metal oxide based sensors.

…